Journal of Infrastructure Preservation and Resilience

CORRECTION Open Access

Correction: Optimizing high-performance fiber-reinforced cementitious composites for improving bridge resilience and sustainability

Xiao Tan[1], Soroush Mahjoubi[1], Qinghua Zhang[2], Daren Dong[3] and Yi Bao[1*]

Correction: J Infrastruct Preserv Resil 3, 18 (2022) https://doi.org/10.1186/s43065-022-00067-0

Following publication of the original article [1], it was found that the wrong article version was published. The original publication has since been corrected. The correct article should be as follows:

Abstract

High-performance fiber-reinforced cementitious composites (HPFRCC) exhibit benefits in improving infrastructure resilience but often compromise sustainability due to the higher upfront cost and carbon footprint compared with conventional concrete. This paper presents a framework to improve bridge resilience and sustainability through optimizing HPFRCC. This research considers ultra-high-performance concrete and strain-hardening cementitious composite, both featuring high mechanical strengths, ductility, and damage tolerance. This paper establishes links between bridge resilience, bridge sustainability, mechanical properties of HPFRCC, and mixture design. The investigated mechanical properties include the first crack stress, the ultimate tensile strength, and the ultimate tensile strain. With the established links, sustainability is maximized while resilience is retained by optimizing HPFRCC mixtures. The framework is implemented into a case study of a bridge that collapsed during construction. Results show that use of HPFRCC enhances resilience, and HPFRCC mixtures can be engineered to minimize the material cost and carbon footprint while retaining high resilience.

Keywords: high-performance fiber-reinforced cementitious composites (HPFRCC); redundancy; optimization; resilience; sustainability; strain-hardening cementitious composite (SHCC); ultra-high-performance concrete (UHPC)

1. Introduction

Bridge collapse continues to occur and causes catastrophic consequences. Bridge collapse is usually attributed to one or a combination of multiple causes [1]: (1) unexpected external effects due to natural and/or anthropogenic events, such as earthquake [2], flood [3], scour [4], fire [5], and collision [6]; (2) material deterioration and lack of maintenance such as steel corrosion [7] and concrete cracks [8]; and (3) inadequate design and/or construction [9, 10]. In concrete bridges, the concrete is cracked as the tensile stress exceeds the first crack stress. Although steel bars are used to enhance the crack resistance, cracks are unavoidable due to many effects such as mechanical loads, shrinkage, and thermal effect. Concrete cracks compromise the serviceability and durability

The original article can be found online at https://doi.org/10.1186/s43065-022-00067-0.

*Correspondence:
Yi Bao
yi.bao@stevens.edu
[1] Department of Civil, Environmental and Ocean Engineering, Stevens Institute of Technology, Hoboken, NJ 07030, USA
[2] Department of Bridge Engineering, Southwest Jiaotong University, Chengdu 610031, Sichuan, China
[3] NY Branch, IH Engineers, P.C., New York, NY 10122, USA

of bridges and increase construction and maintenance expenses [11].

In 2018, a concrete bridge located in Miami, United States, collapsed during construction. The National Transportation Safety Board (NTSB) and Occupational Safety and Health Administration investigated the causes of collapse [12, 13]. The investigation reports indicated that the collapsed bridge lacked redundancy which was defined as "the quality of a bridge that enables it to perform its design function in a damaged state" according to AASHTO LRFD Bridge Design Specifications [14]. Three redundancy pathways have been identified, which are load-path redundancy, structural redundancy, and internal redundancy [15, 16]. The load-path redundancy means that a bridge has multiple load paths, and the failure of one load path does not cause bridge collapse. Structural redundancy exists when damage of one or multiple bridge elements does not fail the load path. The internal redundancy describes that damage of an element does not fail the element. The load-path redundancy focuses on the load path; the structural redundancy focuses on one load path; and the internal redundancy focuses on the elements. Multiple scholars [17-20] investigated the causes of collapse and agreed that the collapsed bridge lacked redundancy.

The incident spurred bridge engineers to re-think the design and construction of bridges, as well as the effective measures to minimize occurrence of collapse. Multiple seminars were held to discuss lessons learned from the catastrophic incident [21, 22]. Intense attention was paid to the use of redundant structural elements and multiple load paths to improve the safety and resilience of bridges, but the fabrication and installation of more elements would also increase the cost and carbon footprint. In fact, the concept of redundancy was known to bridge engineers a long time ago. Indeterminate structures have higher resistance to collapse because the inclusion of redundant elements reduces the sensitivity to damage. However, it is noted that many studies were based on bridges made using conventional concrete, which was weak in tension and had limited internal redundancy. It must be cautious to extend the concept to the scenario where ductile materials are used to fabricate structural elements. For example, steel truss bridges have been proven successful in numerous projects, because steel is a ductile material [16]. It is rational to imagine what would happen if ductile concrete were used to construct the bridge that collapsed in Miami.

High-performance fiber-reinforced cementitious composites (HPFRCC) have demonstrated high ductility and excellent durability under earthquake [23] and fatigue loads [24]. Representative types of HPFRCC include ultra-high-performance concrete (UHPC) [25, 26] and strain-hardening cementitious composites (SHCC) [27, 28]. Both UHPC and SHCC feature high ductility and use chopped fibers to bridge cracks in HPFRCC. Existing studies showed that fibers increased crack resistance and enabled cracked HPFRCC to carry higher loads. UHPC is designed to achieve high mechanical strengths (>120 MPa in compression) by maximizing the particle packing density [29, 30, 31, 32, 33], and SHCC is designed to achieve high ductility (>3% in tension) by tuning fibers, matrix, and fiber-matrix interface [34]. SHCC exhibit multifunctionality such as self-healing [35] and self-cleaning [34]. Self-healing refers to the phenomenon that microcracks in SHCC are filled with hydration products gradually in the presence of moisture [35]. Self-cleaning refers to the capability of decomposing organic dirt via photo-catalytic reactions, which can be imparted into SHCC by incorporating titanium dioxide nanoparticles [34]. Both UHPC and SHCC have been used to construct connections of bridge decks and girders [36, 37].

Previous research showed that the replacement of conventional concrete by UHPC or SHCC improved the crack resistance, flexural strengths, shear strengths, and fatigue life of girders, slabs, columns, and joints [23, 24, 26, 37]. Cracked structural elements were able to carry higher loads before they failed. Based on previous research, it is envisioned that the use of HPFRCC in bridges will enhance their resilience. Fig. 1 illustrates the structural and material pathways of the resilience and sustainability of bridges. It is promising to leverage the

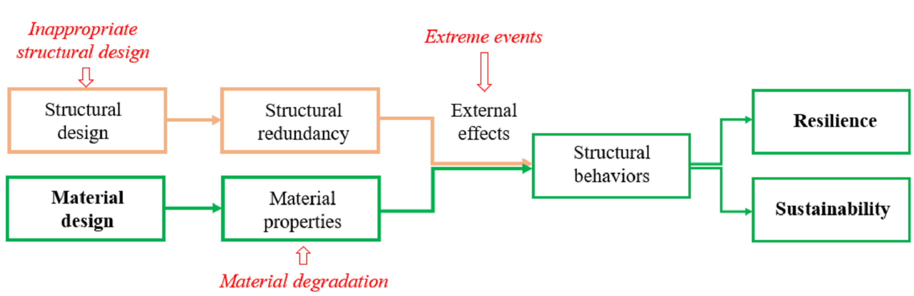

Fig. 1 Illustration of the structural and material pathways to achieve resilience and sustainability

material pathway to supplement the structural pathway in improving bridge resilience.

Meanwhile, HPFRCC is known to involve high upfront material cost [38] and carbon footprint [39], which cause concerns in sustainability. Multiple solutions were proposed to reduce cost and carbon emission. For example, material experts developed cost-effective eco-friendly HPFRCC mixtures using greener raw materials such as industrial by-products, solid wastes, and recycled materials [40-42]. Structural engineers proposed to only utilize HPFRCC at the critical positions of structures such as the connections of bridge decks [36] and joints of buildings [43], while the main bodies of structures were still made using conventional concrete reinforced by steel bars.

Although machine learning models were developed to predict the mechanical properties of HPFRCC [44], existing studies mainly focused on mapping mixture design to material properties. Specifically, two main challenges have been identified from literature: (1) The effects of HPFRCC on the resilience and sustainability of bridges are unclear. Usually, using supplementary materials in mixture design benefits sustainability but shows negative effects on mechanical behaviors. There is a tradeoff between resilience and sustainability. This brings the second challenge. (2) It is unknown how HPFRCC mixtures should be engineered to optimize resilience and sustainability. The challenges are attributed to knowledge gaps in understanding of the effects of the mechanical properties of HPFRCC on bridge behaviors and the lack of effective approaches to optimize the design of HPFRCC mixtures for intended applications.

The overarching goal of this research is to develop a framework to improve bridge resilience and sustainability by using HPFRCC. Specifically, this study has three objectives: (1) to evaluate the effects of key mechanical properties of HPFRCC (i.e., the first crack stresses, ultimate tensile strengths, and ultimate tensile strains of UHPC and SHCC) on the mechanical responses of bridges; (2) to evaluate the resilience of bridges incorporating HPFRCC with different properties; and (3) to develop an effective and efficient approach to enhance material sustainability by optimizing the mixture design of HPFRCC. The development of the approaches is performed based on the bridge that collapsed in Miami in 2018. This research has three technical contributions: (1) A practical framework is proposed to improve bridge resilience and sustainability in terms of the cost and carbon footprint by optimizing HPFRCC mixtures. (2) An innovative pathway of using ductile materials is presented to supplement the pathway of structural redundancy to improve resilience of bridges and to minimize collapse of bridges. (3) A holistic understanding is established on the effects of the mechanical properties of HPFRCC on bridge responses to promote future designs.

2. Methodology

2.1. Overview of the framework

Fig. 2 shows the framework that aims to improve resilience and sustainability via optimizing the mixture design of HPFRCC. The framework is established based on relationships between the design variables and mechanical properties of HPFRCC as well as the relationships between the mechanical properties of HPFRCC and the mechanical responses of bridges. With the bridge responses, resilience and sustainability are evaluated and optimized.

In this research, the link between the design variables and mechanical properties of HPFRCC is established using machine learning predictive models developed in recent research [45-47], and the link between the mechanical properties of HPFRCC and the mechanical responses of bridges is determined via finite element analysis. To stand alone, the machine learning predictive models are briefly introduced in Section 2.2. The finite element analysis approach is presented in Section 2.3. It is envisioned that the framework is applicable to assess bridge resilience and sustainability under various hazards in a life cycle analysis. This research only focuses on the implementation of resilience during bridge construction, as elaborated in Section 2.4. Sustainability mainly considers cradle-to-gate cost and carbon footprint of materials, as presented in Section 2.5.

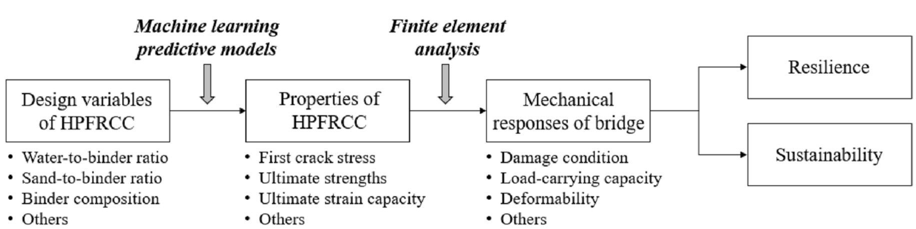

Fig. 2 Illustration of the presented framework to improve bridge resilience and sustainability

2.2. Machine learning predictive models

Different machine learning models were developed to predict the mechanical properties of UHPC and SHCC in recent research [45-47]. To avoid duplication, the predictive models are only briefly introduced herein. The predictive models were machine learning models developed using a large quantity of experimental data of UHPC and SHCC through a "training" process, which was used to establish mathematical high-fidelity relationships between mixture design variables (e.g., water-to-binder ratio, sand-to-binder ratio, binder composition) and mechanical properties (e.g., compressive and tensile strengths, first crack stress, ultimate strain capacity) of HPFRCC [45-47]. With the predictive models, the mechanical properties of HPFRCC mixtures are predictable as long as the mixture design variables are provided. The prediction accuracy was evaluated using different performance metrics as summarized in Table 1. The results indicated that the predictive models achieved high accuracy [45-47].

2.3. Finite element analysis

Three-dimensional finite element analysis was performed to analyze the mechanical responses of bridges with HPFRCC. Compared with conventional concrete, HPFRCC features unique tensile properties. Fig. 3 shows a representative tensile stress-strain curve [48]. HPFRCC bears higher loads after cracks are generated. The curve has three linear segments marked by points O, A, B, and C: (1) O-A: linear elastic stage, (2) A-B: hardening stage, and (3) B-C: descending stage. The stress and strain at point A are the first crack stress and first crack strain, respectively. The stress and strain at point B are the ultimate tensile strength and e ultimate tensile strain, respectively. The strain at point C is the final strain.

Table 1 Performance metrics for predicting HPFRCC mechanical properties [45, 46]

HPFRCC types	Mechanical properties	Dataset	Performance metric			
			MAD	MAE	RMSE	R^2
SHCC	Compressive strength	Training	0.029	0.589	1.901	0.990
		Testing	3.165	4.125	5.478	0.954
	Tensile strength	Training	0.009	0.072	0.176	0.998
		Testing	0.467	0.568	0.731	0.965
	Ductility	Training	0.040	0.105	0.217	0.993
		Testing	0.287	0.507	0.750	0.931
UHPC	Compressive strength	Training	1.380	2.230	3.450	0.990
		Testing	0.940	1.550	2.570	0.990
	Flexural strength	Training	0.560	0.830	1.220	0.970
		Testing	0.860	1.400	1.980	0.940

Note: "MAD" refers to mean absolute deviation; "MAE" refers to median absolute error; "RMSE" refers to root mean squared error; "R^2" refers to coefficient of determination

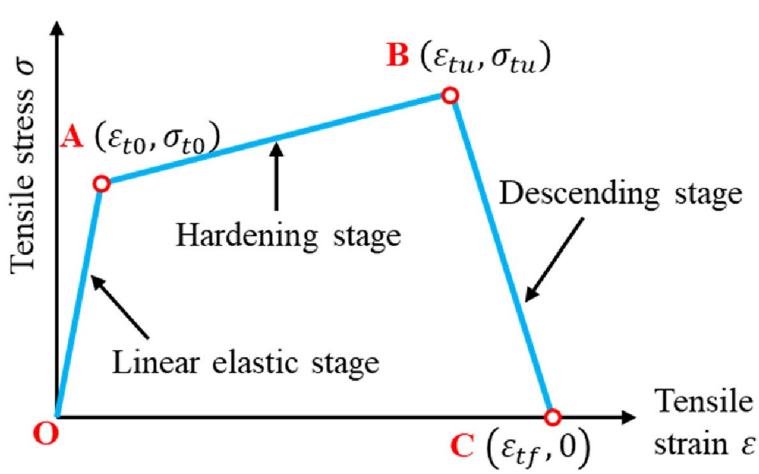

Fig. 3 Illustration of the tensile stress-strain constitutive model of HPFRCC with high ductility

The tensile stress-strain relationship of HPFRCC is formulated as:

$$\sigma = \begin{cases} \frac{\sigma_{t0}}{\varepsilon_{t0}}\varepsilon & , \ 0 \le \varepsilon < \varepsilon_{t0} \\ \sigma_{t0} + (\sigma_{tu} - \sigma_{t0})\left(\frac{\varepsilon - \varepsilon_{t0}}{\varepsilon_{t0} - \varepsilon_{tu}}\right) & , \ \varepsilon_{t0} \le \varepsilon < \varepsilon_{tu} \\ \sigma_{tu}\left(1 - \frac{\varepsilon - \varepsilon_{tu}}{\varepsilon_{tf} - \varepsilon_{tu}}\right) & , \ \varepsilon_{tu} \le \varepsilon < \varepsilon_{tf} \\ 0 & , \ \varepsilon \ge \varepsilon_{tf} \end{cases} \quad (1)$$

where σ and ε are the tensile stress and tensile strain, respectively; ε_{t0} and σ_{t0} are the first crack strain and first crack stress, respectively; ε_{tu} anσ_{tu} are the ultimate tensile strain and ultimate tensile strength, respectively; and ε_{tf} is the final strain.

The first crack stress σ_{t0} is the tensile stress at the elastic limit of HPFRCC [48]. The first crack strain ε_{t0} is the strain corresponding to the first crack stress. First crack stress and first crack strain characterize the crack resistance of HPFRCC. The ultimate tensile strength σ_{tu} is the peak tensile stress. The ultimate tensile strain ε_{tu} is the strain corresponding to the peak tensile stress [48]. The ultimate tensile strength and ultimate tensile strain characterize the post-cracking behavior. The final strain ε_{tf} is the tensile strain of HPFRCC when the tensile stress is reduced to zero. The final strain is a parameter used to control the descending stage in terms of the descending slope. More details of finite element models are elaborated in the case study in Section 3.

2.4. Evaluation of resilience

Various approaches have been proposed to evaluate the resilience of bridges in literature. In this research, resilience is defined as the ability of a bridge to maintain a level of robustness during or after an extreme event, and the ability to return to a desired performance level within the shortest time to minimize the impact on the community, as shown in Fig. 4. This section introduces the key parameters (e.g., the robustness and recovery time) and the quantification of the key parameters.

2.4.1. Robustness

Robustness (P_R) is the residual performance after extreme events and is defined as:

$$P_R = 100\% - f(H, V, U_F, I) = 100\% - \max(9.259 \times H \times V \times U_F) \times I \ge 0\% \quad (2)$$

where H is the hazard value ranging from 1 to 3, which is determined by the severity level of hazards (see details of selection of values of H in Table S1); V is the vulnerability value related to damages in bridges determined by Equation (10); U_F is the uncertainty factor used to consider the uncertainties in bridge assessment as shown in Equation (3); and I is the importance factor of the bridge ranging from 0.75 to 1.25, which is determined by criteria such as bridge location, replacement costs, and average daily traffic (see details of selection of values of I in Tables S2). The value of P_R is normalized to the range of 0 to 100% by a constant 9.259. P_R is calculated to represent the worst scenario as an envelope of all hazard and vulnerability combinations that could possibly cause interruption of performance.

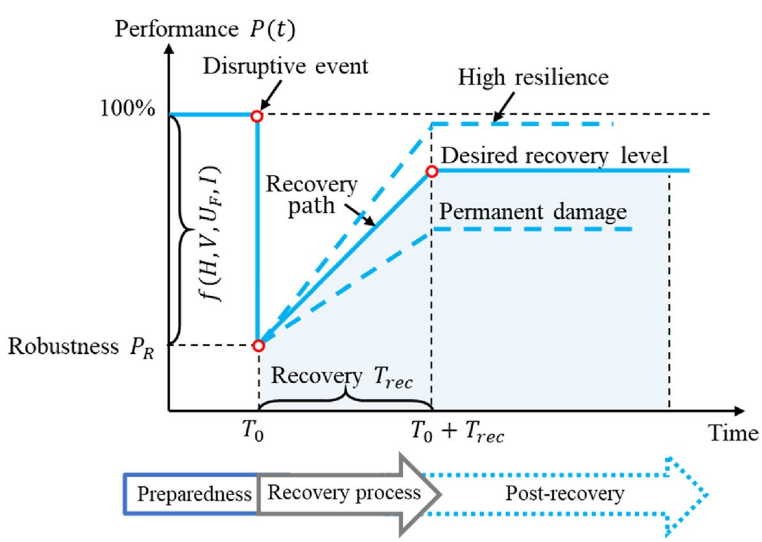

Fig. 4 Conceptual illustration of the resilience of a bridge subjected to a disruptive event

$$U_F = \begin{cases} 1.2, & \text{Visual inspection} \\ 1.1, & \text{Visual inspection and analytical techniques} \\ 1.0, & \text{Visual inspection, analytical, and NDE techniques} \end{cases} \quad (3)$$

2.4.2. Recovery time

The recovery time (T_{rec}) is a function of the basic restoration time and adjustment factors, as shown in Equation (4):

$$T_{rec} = T_{res} \times \alpha_1 \times \alpha_2 \times \alpha_b \quad (4)$$

where T_{rec} is the recovery time; T_{res} is the basic restoration time affected by severity of the hazard and affected area; α_1 is the adjustment factor of disaster management practices ranging from 0.8 to 1.0; α_2 is the adjustment factor of agency's contracting practices ranging from 1.0 to 1.6; and α_b is the adjustment factor of bridge types ranging from 1.00 to 1.50. The details of selection of values of basic restoration time and adjustment factors are determined in Tables S3 to S6.

2.4.3. Resilience

Resilience (R) is calculated as the ratio of the area under the post-disruption performance to the area under the target performance level, as shown in Equation (5). The target performance level is assumed to be 100% over the control time T_{rec}. To compare bridges with regard to their resilience, it is useful to put the calculated value in the context of a discrete ranking system, as suggested in Table S7 in the supplementary material. The thresholds show the ranking method based on resilience value, and they are tailored in intended applications.

$$R = \frac{\int_{T_0}^{T_0+T_{rec}} P(t)dt}{\int_{T_0}^{T_0+T_{rec}} P(100\%)dt} \quad (5)$$

where $P(t)$ is the performance of the bridge; $P(100\%)$ is the performance of the bridge at 100% level (non-interrupted); T_0 is the time (unit in days) when extreme or disruptive events take place.

2.5. Evaluation of sustainability

With the mixture design of HPFRCC, the sustainability of bridge can be evaluated in terms of life-cycle (cradle-to-gate) cost and carbon footprint of all the raw ingredients. The inventory of unit cost and carbon footprint of each ingredient of HPFRCC were presented in references [45-47] and used to calculate the material cost and carbon footprint of HPFRCC by Equations (6) and (7):

$$MC = \sum_{i=0}^{n} m_i \times c_i \quad (6)$$

$$CF = \sum_{i=0}^{n} m_i \times CO_2 - eq_i \quad (7)$$

where MC and CF are the material cost and carbon footprint; n is the number of raw materials; m_i is the mass of i-th raw material in a unit mass of HPFRCC; c_i is the unit price of the i-th raw material; and CO_2-eq_i is the carbon dioxide equivalent of a unit mass of the i-th raw material.

2.6. Multi-objective optimization

With the links between the mixture design variables of HPFRCC and bridge resilience and sustainability, a multi-objective optimization problem is defined to minimize the material cost and carbon footprint while retaining the resilience of bridge through optimizing the mixture design. In other words, bridge resilience is used to define the constraints, and the optimal mixture design is searched to minimize the material cost and carbon footprint. The objective functions and design constraints are formulated to maximize the mechanical properties and minimize the material cost and the carbon footprint of HPFRCC. Two objective functions were considered in the optimization: (1) the minimal material cost; and (2) the minimal carbon footprint.

Four design constraints were imposed to ensure high bridge resilience: (I) CS $\geq \alpha_1$, (II) FCS $\geq \alpha_2$, (III) UTS $\geq \alpha_3$, and (IV) UTN $\geq \alpha_4$, where CS, FCS, UTS, and UTN denote the compressive strength, first crack stress, ultimate tensile strength, and ultimate tensile strain, respectively; and α_i is the lower bound for the i-th design constraints. The lower bounds are determined through performing a parametric study of the mechanical properties of HPFRCC on the bridge resilience based on a finite element analysis. The lowest compressive strength, first crack stress, ultimate tensile strength, and ultimate tensile strain of HPFRCC that lead to high resilience are used to set the lower bounds of the design constraints.

The Non-dominated Sorting Genetic Algorithm II (NSGA-II) [49] was adopted to solve the multi-optimization problem. The algorithm searches for a set of optimal solutions that define the best trade-off between competing objectives. Among the set of design solutions, the optimal mixture designs are selected to achieve high resilience and sustainability. The selection is performed based on the ranking of the design solutions. The ranking of the design solutions is performed using a sustainability index (EI) defined as:

$$EI_i = 1 - 0.5\left[\frac{CF_i - \min(CF)}{\max(CF) - \min(CF)} + \frac{MC_i - \min(MC)}{\max(MC) - \min(MC)}\right] \quad (8)$$

where EI_i is the sustainability index of the i-th mix design; CF_i and MC_i are the carbon footprint and material cost of the i-th mix design, respectively. The

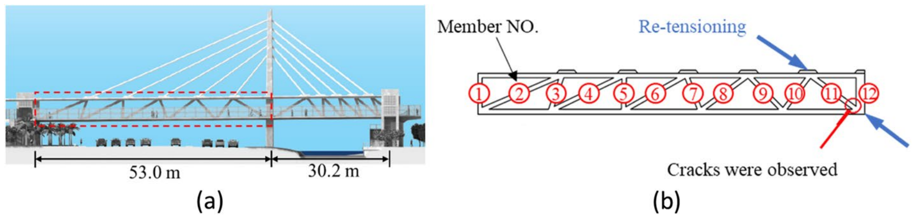

Fig. 5 Illustration of the bridge: (a) rendering of the bridge; and (b) the critical step causing bridge collapse: re-tensioning of the tendons in member 11

sustainability index is between 0 and 1: 0 means the least sustainability, and 1 means the highest sustainability.

3. Case Study

3.1. Bridge description

The bridge was a faux cable-stayed bridge with a determinate prestressed concrete truss girder, as shown in Fig. 5(a). The bridge had two spans, including a 53.0-m main span over an roadway and a 30.2-m canal span [50]. The walkway deck acts as the bottom flange. The roof canopy acts as the top flange. The diagonal struts carry either compression or tension forces, based on angles and positions. An accelerated bridge construction method was adopted to erect the bridge. After the tendons were stressed, a transporter was used to roll the girder into place and set it on the piers.

Before the main span was moved using the transporter, concrete cracks were observed in the nodal region between truss members 11 and 12 before the re-tensioning operation (Fig. 5(b)). With the cracks, the bridge collapsed when tendons in member 11 were re-tensioned. The canal span, access ramps, and faux cable-stay tower were not constructed yet when the bridge collapsed [13].

3.2. Forensic analysis

3.2.1. Nodal region

According to Federal Highway Administration [13], severe underestimation of the demands and overestimation of the capacity of the nodal regions were made in the bridge design, as shown in Fig. 6. Although the nodal region 1-2 between members 1 and 2 had the highest demand-to-capacity ratio, the bridge failed at the nodal region 11-12, because the nodal region 11-12 was framed into a 0.6-m diaphragm, while node region 1-2 was framed into a 1.0-m diaphragm.

In addition, the depth of member 11 was only 67% that of member 2. NTSB concluded that the concrete distress, which was initially observed in nodal region 11-12, was consistent with the underestimation of interface shear demand and the overestimation of identified capacity in the bridge design [13].

3.2.2. Cold joints

The superstructure of the bridge was built offsite through casting concrete three times. The concrete casting resulted in cold joints at each end of the truss members: one end at the bottom of the member (deck-to-member interface), and the other end at the top of the member (member-to-canopy interface), as shown in Fig. 7(a) [13]. In the design of the bridge, multiple drawings pointed out that cold joints need to be roughened to achieve a 6-mm amplitude of roughness [13]. However, the interfaces of cold joints were not properly roughened in real construction, which leads to reduced shear resistance at the interfaces of cold joints, as shown in Fig. 7(b).

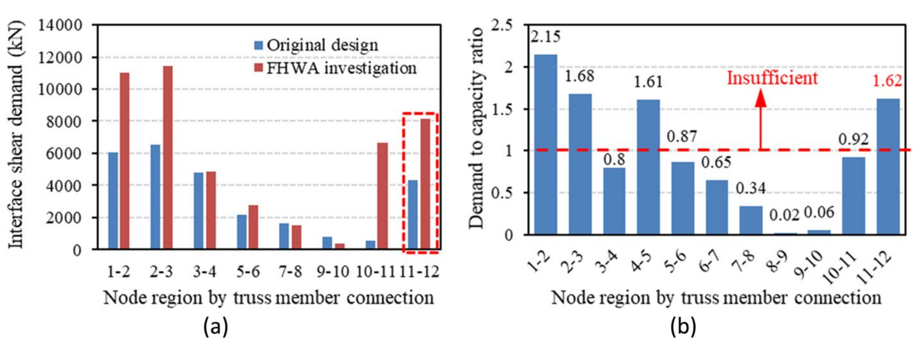

Fig. 6 Underestimation of demands and overestimation of capacity of nodal regions in bridge design [13]: (a) interface shear force demands in the original design and FHWA investigation; and (b) demand to capacity ratios for nodal regions

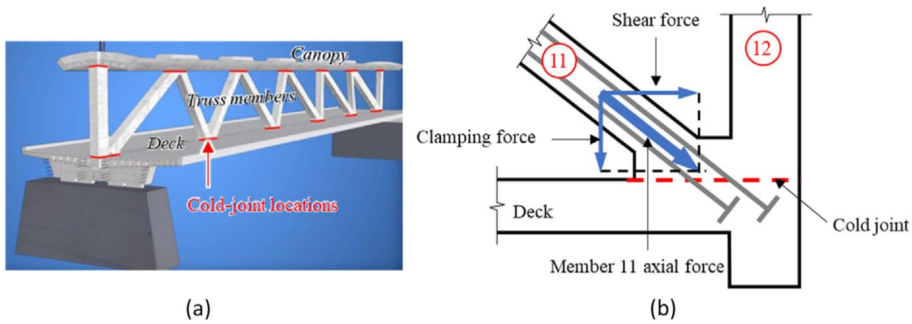

Fig. 7 Cold joints of the truss members: (a) positions of cold joints (image reprinted from OSHA investigation report [12]); and (b) internal force analysis at the 11-12 nodal position

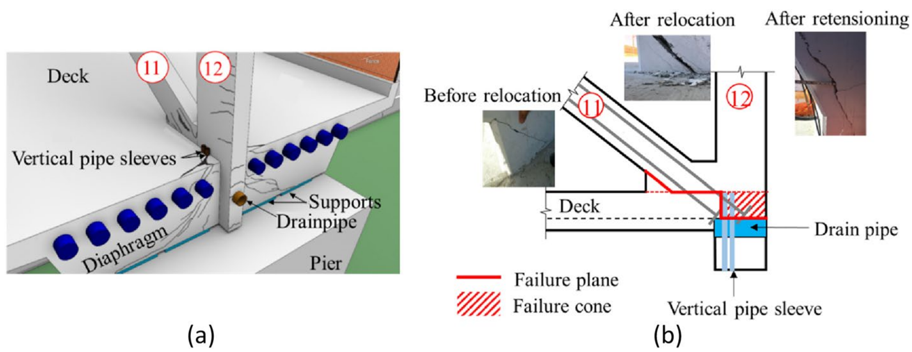

Fig. 8 Development of cracks in the deck and the diaphragm after de-tensioning of member 11: (a) the crack pattern at nodal region 11-12 (image reprinted from NTSB accident report [13]) ; and (b) the evolution of cracks and the failure mechanism of nodal region 11-12

3.2.3. Cracks

The first crack appeared at the nodal region 11-12 when the falsework was removed [12]. Subsequent cracks were produced during transport of the bridge. After the bridge superstructure was supported by the piers, member 11 was de-tensioned according to the construction plan [50]. When member 11 was de-tensioned, more cracks were generated in nodal region 11-12. Fig. 8 shows the development of cracks in the deck and the diaphragm of the bridge after de-tensioning of the tendons in member 11 was completed.

3.2.4. Re-tensioning

After severe cracks were observed from the deck and the diaphragm, tendons in member 11 were re-tensioned. The re-tensioning operation was performed to close the observed cracks, which however increased the shear forces across the interface of cold joints. The increase of shear forces caused failure in the cold joint, which subsequently resulted in the bridge collapse [13]. More details of the collapse process are available in references [11-13, 17-20].

3.3. Finite element model

Fig. 9(a) shows the finite element model established using software ABAQUS [51]. When the bridge collapsed during construction, only the main span was constructed. In this study, only the main span of the bridge was considered in the finite element model. Concrete was modeled using three-dimensional eight-node solid elements with reduced integration (C3D8R). Steel bars and prestressed tendons were modeled using three-dimensional two-node truss elements (T3D2). Steel bars are embedded in concrete. The two ends of prestressed tendons are tied with corresponding anchor plates, which are tied with concrete at the anchorage zones. Prestressing is modeled through initial temperature load, and anchorages at each end of the tendons transfer the prestressed force to the concrete to simulate the post-tensioning effect. A mesh size convergence analysis was performed to determine the appropriate mesh size. The global mesh size was 120 mm, and the mesh size was refined to 60 mm at joints.

The mechanical properties of concrete, steel bars, prestressing tendons, and steel rods adopted in the finite element model were consistent with the realistic bridge [50]. The tensile strength and the compressive strength of the concrete were 2.88 MPa and 58.5 MPa [52], respectively. The elastic modulus and Poisson's ratio were 30.8 GPa and 0.2 [52], respectively. The density was 2,650 kg/m^3 [52]. In simulation of post-cracking behavior of concrete, inelastic concrete properties were applied using

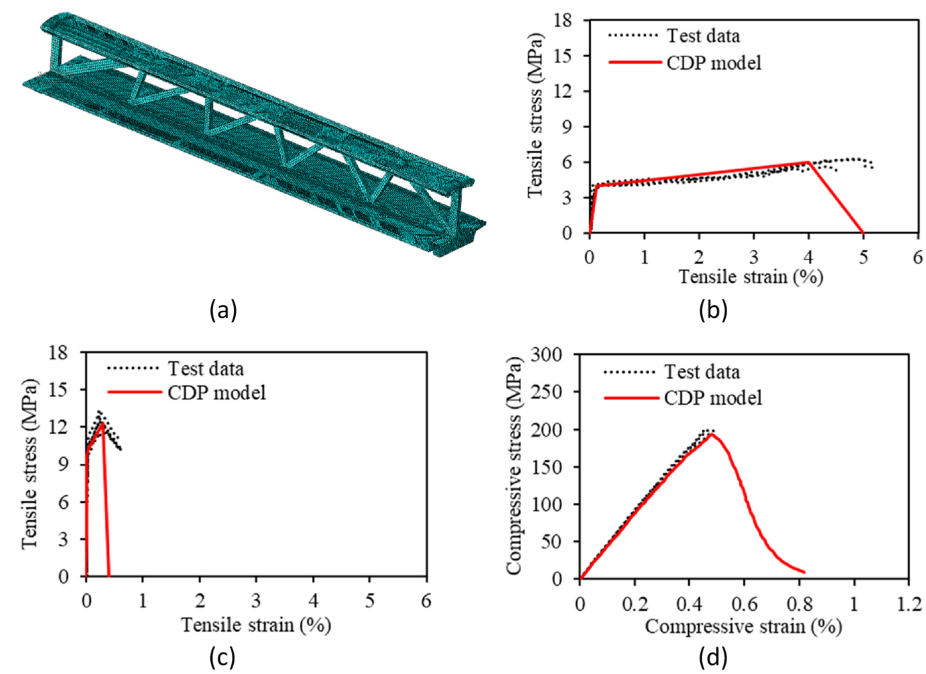

Fig. 9 Finite element model of the bridge: (a) meshed model; (b) tensile properties of SHCC [55]; (c) tensile properties of UHPC [56]; and (d) compressive properties of UHPC [57, 58]

the concrete damage plasticity (CDP) model [53, 54]. The parameters used in the CDP model are listed as follows according to reference [53]: dilatation angle = 30°; eccentricity = 0.1; f_{b0}/f_{c0} = 1.16; K = 0.6667; and viscosity parameter = 0.0005. The dilatation angle and the eccentricity parameter reflect the plastic straining response of the concrete. Parameters f_{b0}/f_{c0} and K determine the shape and the size of the bi-linear yield surface of the concrete.

In this study, UHPC and SHCC are only utilized to replace member 11 and two adjacent joints of member 11 to maximize their effects. Material properties of UHPC and SHCC were determined from test data in references [55-58], as shown in Figs. 9(b) to 9(d). The adopted constitutive relationships are conservative compared with the test data. The properties of SHCC and UHPC used in the CDP model are shown in Table 2. Regarding the compressive properties, this research adopted the same CDP models, and the stress magnitudes were tailored using the compressive strengths of the concrete, SHCC, and UHPC.

Damage initiation criterion and element deletion were defined to reflect tensile damage. For the conventional concrete, the definition of *DAMAGET* is elaborated in references [53, 54]. For SHCC and UHPC, *DAMAGET* is defined as shown in Equation (9):

$$DAMAGET = (\varepsilon - \varepsilon_e)/\left(\varepsilon_{tf} - \varepsilon_e\right) \tag{9}$$

where ε is the tensile strain; ε_e is the elastic strain; ε_{tf} is the final tensile strain; and thus, the value of *DAMAGET* is between 0 to 1. *DAMAGET* is utilized to correlate with vulnerability value (V) in this study using Equation (10):

$$V = \begin{cases} 1, & 0 < DAMAGET \leq 0.25 \\ 2, & 0.25 < DAMAGET \leq 0.6 \\ 3, & 0.6 < DAMAGET \leq 1.0 \end{cases} \tag{10}$$

3.4. Investigated cases

Table 3 lists 22 cases investigated in this study. Case 1 represents the real bridge concrete and is used as the control. There are 11 cases for SHCC, and 10 cases for UHPC. In this study, the investigated material properties were the first crack stress (σ_{t0}), the ultimate tensile strength (σ_{tu}), and the ultimate tensile strain (ε_{tu}).

Table 2 Material properties for SHCC and UHPC [42, 57]

Materials properties	SHCC	UHPC
Density (kg/m^3)	1,800-2,100	2,400-2,600
Elastic modulus (GPa)	15-23	42-55
Poisson's ratio	0.2	0.18
Dilation angle	20°	15°
Eccentricity	0.1	0.1
f_{b0}/f_{c0}	1.16	1.16
K	0.6667	0.6667
Viscosity parameter	0.0005	0.0005

Table 3 Investigated cases

Case	Material	Compressive strength σ_c (MPa)	First crack stress σ_{t0} (MPa)	Ultimate tensile strength σ_{tu} (MPa)	Ultimate tensile strain ε_{tu} (%)
1	Concrete	58.5	-	2.88	0.1
2	SHCC	58.5	2	8	4.0
3	SHCC	58.5	3	8	4.0
4	SHCC	58.5	4	8	4.0
5	SHCC	58.5	5	8	4.0
6	SHCC	58.5	6	8	4.0
7	SHCC	58.5	4	6	4.0
8	SHCC	58.5	4	10	4.0
9	SHCC	58.5	4	12	4.0
10	SHCC	58.5	4	8	6.0
11	SHCC	58.5	4	8	8.0
12	SHCC	58.5	4	8	10.0
13	UHPC	190	8	14	0.3
14	UHPC	190	10	14	0.3
15	UHPC	190	12	14	0.3
16	UHPC	190	14	14	0.3
17	UHPC	190	10	10	0.3
18	UHPC	190	10	12	0.3
19	UHPC	190	10	16	0.3
20	UHPC	190	10	10	0.5
21	UHPC	190	10	10	0.7
22	UHPC	190	10	10	1.0

Equation (11) was developed to relate the first crack stress to the compressive strength of HPFRCC according to ACI 318 [59, 60]:

$$\sigma_{t0} = 0.62 \times \lambda \times \sigma_c{}^{0.5} \tag{11}$$

where σ_c is to compressive strength of HPFRCC (unit in MPa); λ is a constant related to the length of fibers and is calculated by Equation (12):

$$\lambda_{min} \leq \lambda < \lambda_{ave} \tag{12a}$$

$$\lambda_{min} = \begin{cases} 1.0 & \text{, for concrete without fiber} \\ 0.75 & \text{, for HPFRCC with fiber length } (l_f) < 10 \text{ mm} \\ 0.02l_f + 0.1 \leq 1.3 & \text{, for HPFRCC with fiber length } (l_f) \geq 10 \text{ mm} \end{cases} \tag{12b}$$

$$\lambda_{ave} = \begin{cases} 1.0 & \text{, for concrete without fiber} \\ 1.0 & \text{, for HPFRCC with fiber length } (l_f) < 10 \text{ mm} \\ 0.02l_f + 0.4 & \text{, for HPFRCC with fiber length } (l_f) \geq 10 \text{ mm} \end{cases} \tag{12c}$$

where λ_{min} and λ_{ave} are the minimum value and the average value for λ based on data points; and l_f refers to fiber length for HPFRCC.

The ranges of the first crack stresses of SHCC and UHPC were determined using Equations (11) and (12). The first crack strains of SHCC and UHPC mixtures are typically less than 0.1% [61-63]. Regarding SHCC, the investigated first crack stresses were 2 MPa, 3 MPa, 4 MPa, 5 MPa, and 6 MPa; the tensile strengths were 6 MPa, 8 MPa, 10 MPa, and 12 MPa [64]; and the tensile strain capacity values were 4%, 6%, 8%, and 10% [65-67]. Regarding UHPC, the investigated first crack stresses were 8 MPa, 10 MPa, 12 MPa, and 14 MPa [68]; the tensile strengths were 10 MPa, 12 MPa, 14 MPa, and 16 MPa; and the tensile strain capacity values were 0.3%, 0.5%, 0.7%, and 1.0%. Many experimental data showed that UHPC achieved an ultimate tensile strain capacity of 0.3% to 0.5% [69-71]. Some researchers used the ultimate strain capacity of 1% [56, 57], which is possible to achieve but has not been supported by rich experimental data. Therefore, the parametric study on the tensile strength of UHPC is based on the strain capacity of 0.3%.

According to previous research [42], the first crack strain, first crack stress, ultimate tensile strain, and ultimate tensile stress of UHPC are also related to compressive strength and flexural strength, as shown in Equation (13):

$$\sigma_{fl} = 1100 \times \rho \times \left(1 - \frac{R_F}{2.3}\right) \tag{13a}$$

$$E_{uc} = 244.14 \times {\sigma_c}^{0.5} \tag{13b}$$

$$\sigma_{tu} = 0.35 \times \sigma_{fl} \tag{13c}$$

$$\varepsilon_{tu} = \frac{\sigma_{tu}}{E_{uc}} \tag{13d}$$

where σ_c and σ_{fl} refer to the compressive strength (unit: MPa) and the flexural strength (unit: MPa) of UHPC, respectively; ρ refers to the fiber content; R_F refers to the ratio of recycled steel fibers to total fiber content; E_{uc} refers to the hardening modulus of UHPC.

4. Results and Discussions

4.1. Validation of finite element model

Fig. 10 compares the finite element analysis results against real observations from the bridge. Fig. 10(a) shows the finite element analysis results of the maximum principal stress in member 11 before the re-tensioning of the as-built bridge made using conventional concrete. The maximum principal tensile stress near the anchor is larger than 2.88 MPa according to the finite element model. Such results are consistent with the cracks observed from the photo of the real bridge before the re-tensioning operation. After the re-tensioning, the maximum principal stresses around the joints are further increased, revealing that the re-tensioning operation tends to generate cracks in the bridge member made using conventional concrete.

Fig. 10(b) shows that *DAMAGET* around the anchorage area reaches 1.0, indicating that the concrete around the anchorage area loses the tensile load-carrying capacity. The finite element analysis results are compared with the observation of cracks from the real bridge [12]. It is found that the finite element analysis results are consistent with the observations from Figs. 10(c) and 10(d). These results indicate that the finite element model is

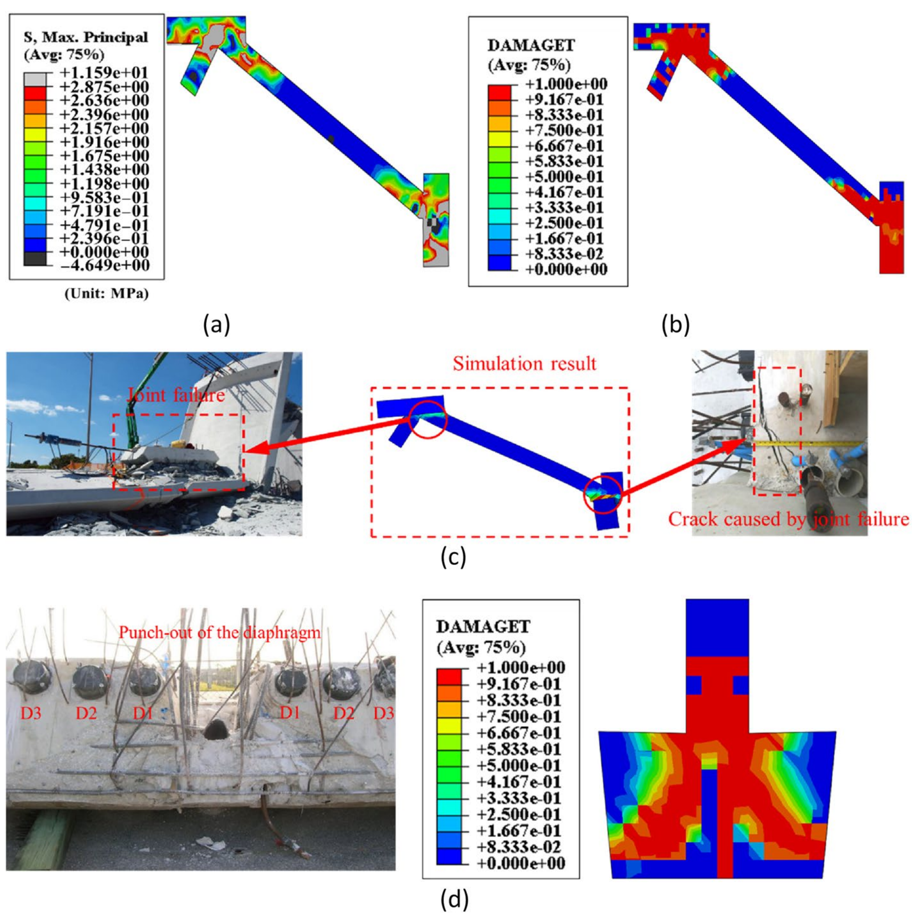

Fig. 10. Analysis results of member 11: (a) contour of the maximum principal stress before the re-tensioning of member 11 (unit: MPa); (b) contour of *DAMAGET* before the re-tensioning of member 11; (c) failure mode of the bridge after the re-tensioning of member 11; and (d) tensile damage of the diaphragm after re-tensioning of member 11

able to reasonably predict the bridge responses under mechanical effects. Therefore, the finite element model is utilized to predict the internal stresses in the bridge.

Another observation from the above analysis is that the collapse of the bridge is closely related to the tensile damage in member 11 and its nodal regions. Therefore, the following analysis mainly focuses on member 11 and its nodal regions at the two ends of the member.

4.2. Bridge resilience

The approach in Section 2.4 was used to determine the values of hazard (H), vulnerability (V), uncertainty (U_F), importance (I), and recovery time for post-extreme event restoration (T_{rec}). The bridge was located in a 100-year flood plain ($H=3$) with high hurricane risk ($H=3$) and was located within 80 km of the coast ($H=3$). The bridge spanned over a busy city street with an annual average daily traffic (ADTT) of 48,500 ($H=3$) based on 2017-2018 data, and the bridge carried no history of overload trucks ($H=1$). Seismicity of the region is seismic design category A ($H=1$), with no record of significant earthquake ($H=1$). The *DAMAGET* of the bridge reached 1 ($V=3$). U_F is assumed to be 1.2 because only visual inspection information was used. The bridge was not located on the Strategic Highway Network (STRAHNET), and it is a pedestrian bridge with no ADTT. Therefore, the importance factor of the bridge (I) is 1. Robustness of the bridge is calculated as:

$$P_R = 100\% - \max\left(9.259 \times H \times V \times U_F\right) \times I = 0\% \tag{14}$$

The bridge collapsed on March 15, 2018, and the road was closed until March 24, 2018, when the debris was cleaned. The severity of the hazard was moderate for an isolated hazard, and the basic extreme event time (T_{res}) was 2 weeks. It is assumed that the agency did not meet extreme event management practices ($\alpha_1=1.0$). Also, there was no history of extreme events in the year before 2018 ($\alpha_2=1.0$). The bridge type was single span ($\alpha_b=1.0$). Therefore, the recovery time for the bridge is calculated as:

$$T_{rec} = T_{res} \times \alpha_1 \times \alpha_2 \times \alpha_b = 14 \text{ days} \tag{15}$$

Based on the robustness and recovery time, the resilience of the bridge is calculated as:

$$R = \frac{\int_{T_0}^{T_0+T_{rec}} P(t)dt}{\int_{T_0}^{T_0+T_{rec}} P(100\%)dt} = \frac{0.5 \times 14 \times 100}{14 \times 100} = 50\% \tag{16}$$

According to the proposed resilience classification (see Table S7), this bridge is classified in the low-resilience category, which is aligned with the identified level of damage (complete failure) and is validated against the damage source for the bridge collapse: Lack of redundancy.

4.3. Parametric study results

Fig. 11 compares the tensile damage distributions in member 11 when it is made with different materials (i.e., conventional concrete, SHCC, and UHPC) and subject to re-tensioning. When the conventional concrete is used, the two joints of member 11 are severely damaged, as indicated by the results of *DAMAGET* reaching 1.0 in Fig. 11(a). Major cracks were caused and developed beyond the anchorage zone of the tendons in the deck. When the SHCC is used, the severity of damage at the two joints of member 11 is highly alleviated as shown in Fig. 11(b). Member 11 is expected to exhibit densely-distributed microcracks under tension. The damage tolerance of SHCC makes the member just slightly damaged at joints under the same load condition. When the UHPC is used, there is minor damage in member 11, as shown in Fig. 11(c). The different damage conditions are associated with the different mechanical properties, in particular, the first crack stress, the tensile strength and strain capacity of the different materials. The results indicate that using HPFRCC in critical joints or members

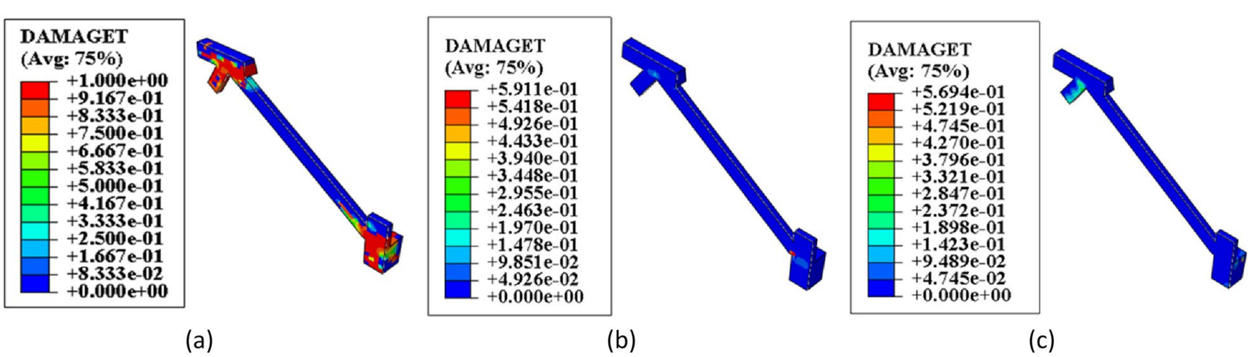

Fig. 11. Contours of tensile damage distributions of member 11 made using different materials: (a) conventional concrete; (b) SHCC ($\sigma_{t0} = 4$ MPa; $\varepsilon_{tu} = 4\%$; $\sigma_{tu} = 8$ MPa); and (c) UHPC ($\sigma_{t0} = 10$ MPa; $\varepsilon_{tu} = 0.3\%$; $\sigma_{tu} = 14$ MPa)

decreases the level of tensile damage. It is envisioned that the resilience value and category of the investigated bridge will be significantly improved with proper mechanical properties of HPFRCC, as elaborated in parametric studies in Section 4.3.

4.3.1. Effect of first crack stress

Fig. 12 shows the results of effect of first crack stress on the maximum tensile damage and resilience. Fig. 12(a) shows that as the first crack stress of SHCC increases, the maximum tensile damage (*DAMAGET*) decreases, and the resilience value increases. If the SHCC has an ultimate tensile strain of 4% and an ultimate tensile strength of 8 MPa, which are conservative according to the published papers [64-67], as the first crack stress increases from 2 MPa to 6 MPa, the tensile damage decreases from 0.82 to 0.30, and the resilience increases from 50% to 67%.

Fig. 12(b) shows that with the increase of first crack stress of UHPC, the maximum tensile damage decreases, and the resilience value increases. If the UHPC has an ultimate tensile strain of 0.3% and an ultimate tensile strength of 14 MPa, which is conservative according to the published papers [68-71], when the first crack stress is increased from 8 MPa to 14 MPa, the tensile damage is reduced from 0.38 to 0.05, which is smaller than 0.30 for the SHCC shown in Fig. 12(a), and UHPC with a *DAMAGET* of 0.05 behaves like uncracked UHPC in terms of the load-carrying capability and long-term durability [72]; the resilience value is increased from 67% to 83%, and resilience class of UHPC at $R = 83\%$ is high.

4.3.2. Effect of ultimate tensile strength

Fig. 13 shows the effect of the ultimate tensile strength on the maximum tensile damage and resilience. In Fig. 13(a), the SHCC has a first crack stress of 4 MPa and ultimate tensile strain of 4%, which is conservative according to the published papers [64-67]. As the ultimate tensile strength of SHCC increases from 6 MPa to 12 MPa, the maximum tensile damage decreases from 1 to 0.027, and the resilience increases from 50% to 83%. For cracked SHCC with *DAMAGET* equal to 0.027, it behaves like uncracked SHCC in terms of the load-carrying capability and long-term durability according to reference [72].

In Fig. 13(b), the UHPC has a first crack stress of 10 MPa and an ultimate tensile strain of 0.3%, which is conservative according to the published papers [68-71]. As

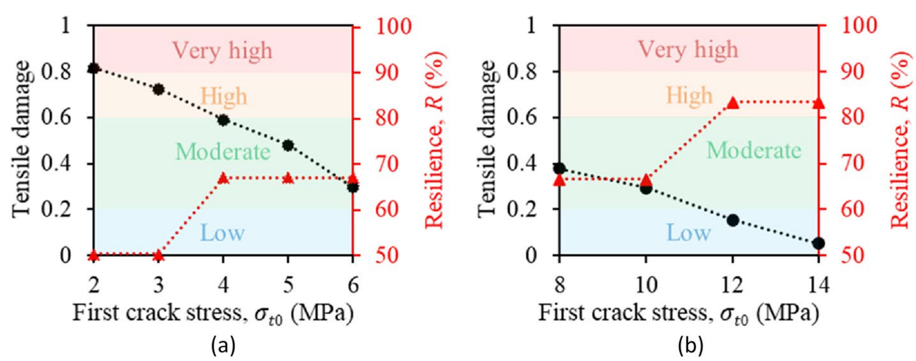

Fig. 12. The effect of the first crack stress on the maximum tensile damage and resilience: (a) SHCC ($\varepsilon_{tu} = 4\%$ and $\sigma_{tu} = 8$ MPa); and (b) UHPC ($\varepsilon_{tu} = 0.3\%$ and $\sigma_{tu} = 14$ MPa)

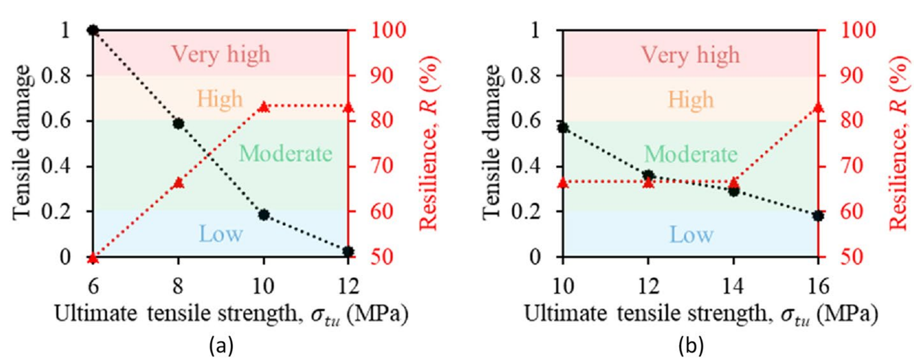

Fig. 13. The effect of the ultimate tensile strength on the maximum tensile damage and resilience: (a) SHCC ($\sigma_{t0} = 4$ MPa and $\varepsilon_{tu} = 4\%$); and (b) UHPC ($\sigma_{t0} = 10$ MPa and $\varepsilon_{tu} = 0.3\%$)

the ultimate tensile strength increases from 10 MPa to 16 MPa, the maximum tensile damage decreases from 0.57 to 0.18, and the resilience increases from 67% to 83%. The *DAMAGET* is higher than 0.027 of the SHCC in Fig. 13(a) because *DAMAGET* is defined based on the tensile strain, and the UHPC has a lower tensile strain capacity than the SHCC as shown in Fig. 9.

4.3.3. Effect of ultimate tensile strain

Fig. 14 shows the effect of the ultimate tensile strain on the maximum tensile damage and resilience. In Fig. 14(a), the SHCC has a first crack stress of 4 MPa and an ultimate tensile strength of 8 MPa, which is conservative according to the published papers [64-67]. As the ultimate tensile strain increases from 4% to 10%, the maximum tensile damage decreases from 0.59 to 0.23, and the resilience increases from 67% to 83%. In Fig. 14(b), the UHPC has a first crack stress of 10 MPa and an ultimate tensile strength of 10 MPa, which is conservative according to the published papers [68-71]. As the ultimate tensile strain increases from 0.3% to 1%, the maximum tensile damage decreases from 0.57 to 0.15, and the resilience increases from 67% to 83%.

4.3.4. Summary

The results indicate that the use of UHPC and SHCC is able to decrease the tensile damage at the critical locations of the bridge. Since the tensile damage is the main cause of the collapse of the bridge, the resilience of the bridge is enhanced. Table 4 summarized the resilience results based on the parametric study. The high resilience suggests that the use of UHPC or SHCC will likely avoid the collapse. The parametric study reveals the benefits of increasing the tensile strength and ductility of the ductile materials and provides data to guide the design of the materials and the structures made using the ductile materials.

4.4. Optimization results

A number of candidate solutions are selected based on the results presented in Section 4.3, as listed in Table 5. High resilience is achieved by using mixtures with compressive strengths higher than 58.5 MPa, first crack stresses higher than 4 MPa, ultimate tensile strengths higher than 8 MPa, and ultimate tensile strains more than 4%. The sustainability index of each mixture is reported in Table 5. The results indicate that mixture S1 is the most cost-effective and eco-friendly mixture with a sustainability index of 0.89.

4.5. Discussion

The optimization results in Table 5 are consistent with the defined performance objectives and design scenarios and also reveal the complexity of optimal design of HPFRCC due to complicated coupling effects among the wide range of mixture design variables. The proposed framework for multi-objective optimization reflects the significance of data-driven solutions with high efficiency and accuracy. The candidate solutions can be validated by a reduced number of experimental tests, which tremendously saves the time and cost of implementation and therefore facilitates efficient development process of HPFRCC. Besides, the candidate solutions provided in this study are also convenient for practical engineers to implement for intended applications of HPFRCC.

5. Conclusions

This research presents a framework for simultaneous enhancement of the resilience and the sustainability of bridges using HPFRCC through optimizing the mixture. The research framework is demonstrated by using UHPC and SHCC based on a collapsed bridge. The collapse process and mechanisms are discussed. The performance of the bridge using SHCC and UHPC is tested, and a parametric study is conducted to understand the effect of tensile behaviors of SHCC and UHPC on the mechanical response and resilience of the bridge. Results show that HPFRCC mixtures can be engineered to minimize the material cost and carbon footprint while retaining high resilience. Based on the investigations, the following conclusions are drawn.

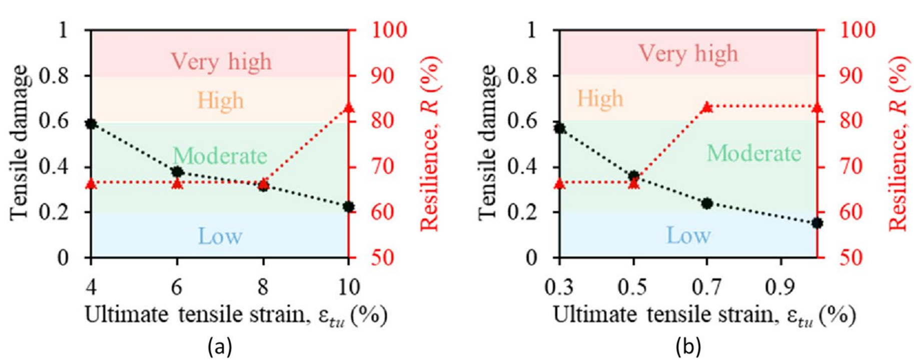

Fig. 14. The effect of tensile strain capacity on the maximum tensile damage and resilience: (a) SHCC (σ_{t0} = 4 MPa and σ_{tu} = 8 MPa); (b) UHPC (σ_{t0} = 10 MPa and σ_{tu} = 10 MPa)

Table 4 Summarization of resilience results in parametric study

Case	Material	Compressive strength (MPa)	First crack stress (MPa)	Ultimate tensile strength (MPa)	Ultimate tensile strain (%)	Resilience (%)	Resilience class
1	Concrete	58.5	-	2.88	0.1	50	Low
2	SHCC	58.5	2	8	4.0	50	Low
3	SHCC	58.5	3	8	4.0	50	Low
4	SHCC	58.5	4	8	4.0	67	Moderate
5	SHCC	58.5	5	8	4.0	67	Moderate
6	SHCC	58.5	6	8	4.0	67	Moderate
7	SHCC	58.5	4	6	4.0	50	Low
8	SHCC	58.5	4	10	4.0	83	High
9	SHCC	58.5	4	12	4.0	83	High
10	SHCC	58.5	4	8	6.0	67	Moderate
11	SHCC	58.5	4	8	8.0	67	Moderate
12	SHCC	58.5	4	8	10.0	83	High
13	UHPC	190	8	14	0.3	67	Moderate
14	UHPC	190	10	14	0.3	67	Moderate
15	UHPC	190	12	14	0.3	83	High
16	UHPC	190	14	14	0.3	83	High
17	UHPC	190	10	10	0.3	67	Moderate
18	UHPC	190	10	12	0.3	67	Moderate
19	UHPC	190	10	16	0.3	83	High
20	UHPC	190	10	10	0.5	67	Moderate
21	UHPC	190	10	10	0.7	83	High
22	UHPC	190	10	10	1.0	83	High

- The presented framework is able to simultaneously optimize the mechanical properties, material costs, and carbon footprint of HPFRCC for bridge resilience and sustainability. The optimization of mixture design of HPFRCC enables the bridge to achieve the minimal material cost and carbon footprint while remaining high resilience.
- The proposed pathway to alleviating damage in bridges and enhancing the resistance to collapse under extreme loading conditions is promising. Regarding the considered bridge example, when the conventional concrete is replaced by UHPC or SHCC, tensile damage was reduced from "significant" to "minor".
- The tensile properties of UHPC and SHCC have large effects on the damage condition. The damage index decreases with the increase of the first crack stress, tensile strength, tensile strain capacity, and ultimate strain capacity. The parametric study provides useful data to guide the design of HPFRCC for bridge applications.
- The investigated bridge collapse was associated with concrete cracks. For bridge collapse controlled by tensile damage, the use of ductile materials is capable of greatly improving safety and resilience. Adoption of ductile materials allows bridge engineers to design bridges with thin elements while retaining the load-carrying capacity.

Based on this research, the following opportunities are identified for future research:

- This study tests the feasibility of the proposed framework to improve bridge resilience and sustainability through optimizing structural materials. The effect of HPFRCC on the life-cycle cost and long-term durability remains unknown. Further research is necessary to uncover the effect and reduce the life-cycle cost and improve durability. Self-healing properties should be considered.
- This study focuses on the construction stages until the bridge collapsed. Although the use of HPFRCC is promising to avoid bridge collapse, it is unclear whether collapse will occur at a later stage. The whole lifecycle needs to be considered in future research to gain a holistic understanding of the safety and resiliency of bridges.

Table 5 Optimal design of HPFRCC mixtures

Mix design	S1	S2	S3	S4	S5	S6	S7	S8	S9
Design variables									
Cement-to-binder ratio	14.4	25.0	25.0	11.8	16.1	16.1	11.8	24.9	25.0
Fly ash-to-binder ratio	27.1	28.4	28.4	20.5	30.8	30.8	27.2	27.0	28.4
Slag-to-binder ratio	7.2	7.2	7.3	7.5	6.8	6.8	6.6	7.4	7.1
Rice husk-to-binder ratio	5.2	9.5	9.4	6.0	17.2	17.2	5.4	16.9	9.3
Limestone-to-binder ratio	40.4	7.2	7.2	43.1	9.0	9.0	43.1	1.6	7.2
Metakaolin-to-binder ratio	4.7	4.9	4.9	9.4	12.5	12.5	3.8	5.1	4.9
Silica fume-to-binder ratio	1.0	17.0	16.8	0.3	6.7	6.7	0.5	16.3	16.8
Sand-to-binder ratio	0.8	0.7	0.8	1.3	0.6	0.6	1.4	0.4	1.4
Water-to-binder ratio	0.2	0.3	0.2	0.2	0.2	0.2	0.2	0.2	0.1
Superplasticizer content (%)	2.0	1.9	1.3	2.0	2.6	2.6	1.8	1.9	1.4
Fiber volume (%)	2.7	2.7	2.8	1.7	2.7	2.7	2.6	2.7	2.7
Fiber length (mm)	18	12	11	27	12	12	27	12	27
Fiber diameter (μm)	24	17	17	40	16	16	40	17	40
Elastic modulus of fibers (GPa)	100	6	6	200	6	6	200	6	200
Fiber type	PE[1]	PP[2]	PP	Steel	PP	PP	Steel	PP	Steel
Output variables									
Compressive strength (MPa)	59.1	62.5	67.3	93.1	103.3	103.2	70.9	114.1	102.6
First crack stress (MPa)	4.8	4.9	5.1	5.6	5.7	5.7	4.9	5.0	5.3
Ultimate tensile strength (MPa)	16.6	14.0	17.2	9.4	10.0	10.0	14.1	11.6	13.2
Ultimate tensile strain (%)	6.0	7.1	4.2	8.5	10.0	10.0	6.1	4.2	8.0
Carbon footprint (kg/m^3)	745	1142	1207	895	1943	1990	1010	2249	1485
Cost (USD/m^3)	633	456	458	872	566	579	1143	610	1292
Sustainability index	0.89	0.87	0.84	0.7	0.54	0.51	0.5	0.41	0.25

[1] PE stands for polyethylene fiber; [2]PP stands for polypropylene fiber

- This study proposes to utilize HPFRCC to replace conventional concrete in a critical member and its joints of the investigated bridge. However, the effect of the length of the joints replaced using HPFRCC on the resiliency and sustainability of the bridge remains unknown. Further research needs to be conducted to systematically evaluate the effect and optimize the joint length.

References

[1] Lee, G. C., Mohan, S., Huang, C., and Fard, B. N. (2013). *A Study of US Bridge Failures (1980-2012)*. MCEER Buffalo, NY. https://www.eng.buffalo.edu/mceer-reports/13/13-0008.pdf. Accessed October 1, 2022.

[2] Akiyama, M., Frangopol, D.M. and Ishibashi, H. (2020). "Toward life-cycle reliability-, risk-and resilience-based design and assessment of bridges and bridge networks under independent and interacting hazards: emphasis on earthquake, tsunami and corrosion." *Structure and Infrastructure Engineering*, 16(1), pp.26-50. https://doi.org/10.1080/15732479.2019.1604770

[3] Khandel, O., and Soliman, M. (2019). "Integrated framework for quantifying the effect of climate change on the risk of bridge failure due to floods and flood-induced scour." *Journal of Bridge Engineering*, 24(9), p.04019090. https://doi.org/10.1061/(ASCE)BE.1943-5592.0001473

[4] Scattarreggia, N., Salomone, R., Moratti, M., Malomo, D., Pinho, R., and Calvi, G. M. (2022). "Collapse analysis of the multi-span reinforced concrete arch bridge of Caprigliola, Italy." *Engineering Structures*, 251, p.113375. https://doi.org/10.1016/j.engstruct.2021.113375

[5] Nicoletta, B., Kotsovinos, P. and Gales, J. (2020). "Review of the fire risk, hazard, and thermomechanical response of bridges in fire." *Canadian Journal of Civil Engineering*, 47(4), pp.363-381. https://doi.org/10.1139/cjce-2018-0767

[6] Deng, L., Wang, W. and Yu, Y. (2016). "State-of-the-art review on the causes and mechanisms of bridge collapse." *Journal of Performance of Constructed Facilities*, 30(2), p.04015005. https://doi.org/10.1061/(ASCE)CF.1943-5509.0000731

[7] Shi, X., Xie, N., Fortune, K. and Gong, J., (2012). "Durability of steel reinforced concrete in chloride environments: An overview." *Construction and Building*

Materials, 30, pp.125-138. https://doi.org/10.1016/j.conbuildmat.2011.12.038

[8] Swenson, D. V., and Ingraffea, A. R. (1991). "The collapse of the Schoharie Creek Bridge: a case study in concrete fracture mechanics." *In Current Trends in Concrete Fracture Research*, pp. 73-92. Springer, Dordrecht. https://doi.org/10.1007/978-94-011-3638-9_6

[9] Hao, S. (2014). "Minnesota I-35W steel bridge collapse: Lessons learned and challenges revealed." *International Journal of Forensic Engineering*, 2(1), 29-70. https://doi.org/10.1504/IJFE.2014.059245

[10] Sacconi, S., Ierimonti, L., Venanzi, I. and Ubertini, F., (2021). "Life-cycle cost analysis of bridges subjected to fatigue damage." *Journal of Infrastructure Preservation and Resilience*, 2(1), pp.1-13. https://doi.org/10.1186/s43065-021-00040-3

[11] Khan, M. and Ali, M., (2016). "Use of glass and nylon fibers in concrete for controlling early age micro cracking in bridge decks." *Construction and Building Materials*, 125, pp.800-808. https://doi.org/10.1016/j.conbuildmat.2016.08.111

[12] Occupational Safety and Health Administration. (2019). "Investigation of March 15, 2018 pedestrian bridge collapse at Florida International University, Miami, FL." https://www.osha.gov/doc/engineering/pdf/2019_r_03.pdf. Accessed January 11, 2022.

[13] National Transportation Safety Board. (2019). "Pedestrian bridge collapse over SW 8th Street, Miami, Florida, March 15, 2018." Highway Accident Report NTSB/HAR-19/02 PB2019-101363. https://www.ntsb.gov/investigations/AccidentReports/Reports/HAR1902.pdf. Accessed January 11, 2022.

[14] Ghosn, M., Yang, J., Beal, D., and Sivakumar, B. (2014). "Bridge system safety and redundancy. (No. NCHRP REPORT 776)" *National Cooperative Highway Research Program (NCHRP)*, Transportation Research Board, United States. https://doi.org/10.17226/22365. Accessed January 22, 2022.

[15] Mertz, D. R. (2012). "Steel Bridge Design Handbook: Redundancy. (No. FHWA-IF 12-052 - Vol. 9)" *Office of Bridges and Structures*, Federal Highway Administration, United States. https://rosap.ntl.bts.gov/view/dot/42893. Accessed January 22, 2022.

[16] Khan, M. A. (2014). *Accelerated Bridge Construction: Best Practices and Techniques*. Elsevier. https://doi.org/10.1016/C2011-0-08185-1

[17] Cao, R., El-Tawil, S., and Agrawal, A. K. (2020). "Miami pedestrian bridge collapse: computational forensic analysis." *Journal of Bridge Engineering*, 25(1), p.04019134. https://doi.org/10.1061/(ASCE)BE.1943-5592.0001532

[18] Zhou, X., Di, J., and Tu, X. (2019). "Investigation of collapse of Florida International University (FIU) pedestrian bridge." *Engineering Structures*, 200, p.109733. https://doi.org/10.1016/j.engstruct.2019.109733

[19] Peng, W., Ding, R., Xu, W., Xu, X., Dai, F., and Taciroglu, E. (2019). "A forensic analysis of the Florida International University pedestrian bridge collapse using incident video footages." *Engineering Structures*, 200, p.109732. https://doi.org/10.1016/j.engstruct.2019.109732

[20] Jiang, L., Ye, J., and Zheng, H. (2019). "Collapse mechanism analysis of the FIU pedestrian bridge based on the improved structural vulnerability theory (ISVT)." *Engineering Failure Analysis*, 104, pp.1064-1075. https://doi.org/10.1016/j.engfailanal.2019.06.033

[21] Klein, G. J. and Phipps, A. R. (2020) " FIU pedestrian bridge collapse: Testing of full size replicas of failed connection." https://seaotdallas.org/event-3879520. Accessed January 11, 2022.

[22] Engineering ethics: The collapse of the FIU pedestrian bridge, design & ethical failures. (2021). https://www.pdhsource.com/course/live-webinar-engineering-ethics-the-collapse-of-the-fiu-pedestrian-bridge/. Accessed January 11, 2022.

[23] Li, X., Wang, J., Bao, Y., and Chen, G. (2017). "Cyclic behavior of damaged reinforced concrete columns repaired with high-performance fiber-reinforced cementitious composite." *Engineering Structures*, 136, pp.26-35. https://doi.org/10.1016/j.engstruct.2017.01.015

[24] Liu, Y., Zhang, Q., Meng, W., Bao, Y., and Bu, Y. (2019). "Transverse fatigue behaviour of steel-UHPC composite deck with large-size U-ribs." *Engineering Structures*, 180, pp.388-399. https://doi.org/10.1016/j.engstruct.2018.11.057

[25] Meng, W., and Khayat, K. H. (2016). "Mechanical properties of ultra-high-performance concrete enhanced with graphite nanoplatelets and carbon nanofibers." *Composites Part B: Engineering*, 107, pp.113-122. https://doi.org/10.1016/j.compositesb.2016.09.069

[26] Meng, W., Khayat, K.H., and Bao, Y. (2018). "Flexural behaviors of fiber-reinforced polymer fabric reinforced ultra-high-performance concrete panels", *Cement and Concrete Composites*, 93, pp.43-53. https://doi.org/10.1016/j.cemconcomp.2018.06.012

[27] Huang, B.T., Yu, J., Wu, J.Q., Dai, J.G. and Leung, C.K., (2020). "Seawater sea-sand Engineered Cementitious Composites (SS-ECC) for marine and coastal applications." *Composites Communications*, 20, p.100353. https://doi.org/10.1016/j.coco.2020.04.019

[28] Huang, B.T., Wang, Y.T., Wu, J.Q., Yu, J., Dai, J.G. and Leung, C.K., (2021). "Effect of fiber content on mechanical performance and cracking characteristics of ultra-high-performance seawater sea-sand concrete (UHP-SSC)." *Advances in Structural Engineering*, 24(6), pp.1182-1195. https://doi.org/10.1177/1369433220972452

[29] Meng, W., Valipour, M., and Khayat, K. H. (2017). "Optimization and performance of cost-effective ultra-high performance concrete." *Materials and Structures*, 50(1), p.29. https://doi.org/10.1617/s11527-016-0896-3

[30] Prejs, A., Jawdhari, A. and Fam, A., (2022). "Pull-out strength of post-installed connectors in thin UHPC members." *Thin-Walled Structures*, 181, p.110023. https://doi.org/10.1016/j.tws.2022.110023

[31] Kadhim, M.M., Jawdhari, A., Nadir, W. and Cunningham, L.S., (2022). "Behaviour of RC beams strengthened in flexure with hybrid CFRP-reinforced UHPC overlays." *Engineering Structures*, 262, p.114356. https://doi.org/10.1016/j.engstruct.2022.114356

[32] Kadhim, M.M., Jawdhari, A. and Peiris, A., (2021). "Development of hybrid UHPC-NC beams: A numerical study." *Engineering Structures*, 233, p.111893. https://doi.org/10.1016/j.engstruct.2021.111893

[33] Jawdhari, A. and Fam, A., (2020). "Thermal-structural analysis and thermal bowing of double Wythe UHPC insulated walls." *Energy and Buildings*, 223, p.110012. https://doi.org/10.1016/j.enbuild.2020.110012

[34] Xu, M., Bao, Y., Wu, K., Xia, T., Clack, H. L., Shi, H., and Li, V. C. (2019). "Influence of TiO_2 incorporation methods on NO_x abatement in engineered cementitious composites." *Construction and Building Materials*, 221, pp.375-383. https://doi.org/10.1016/j.conbuildmat.2019.06.053

[35] Herbert, E.N. and Li, V.C., (2013). "Self-healing of microcracks in engineered cementitious composites (ECC) under a natural environment." *Materials*, 6(7), pp.2831-2845. https://doi.org/10.3390/ma6072831

[36] Du, J., Meng, W., Khayat, K.H., Bao, Y., Guo, P., Lyu, Z., Abu-obeidah, A., Nassif, H. and Wang, H., 2021. New development of ultra-high-performance concrete (UHPC). *Composites Part B: Engineering*, 224, p.109220. https://doi.org/10.1016/j.compositesb.2021.109220

[37] Lepech, M. D., and Li, V. C. (2009). "Application of ECC for bridge deck link slabs." *Materials and Structures*, 42(9), pp.1185-1195. https://doi.org/10.1617/s11527-009-9544-5

[38] Lu, K., Xu, Q., Li, W., Hu, Y., Wang, J. and Yao, Y., (2021). "Fatigue performance of UHPC bridge deck system with field-cast dovetail joint." *Engineering Structures*, 237, p.112108. https://doi.org/10.1016/j.engstruct.2021.112108

[39] Guo, P., Meng, W., Xu, M., Li, V. C., and Bao, Y. (2021). "Predicting mechanical properties of high-performance fiber-reinforced cementitious composites by integrating micromechanics and machine learning." *Materials*, 14(12), p.3143. https://doi.org/10.3390/ma14123143

[40] Du, J., Liu, Z., Christodoulatos, C., Conway, M., Bao, Y., and Meng, W. (2022). "Utilization of off-specification fly ash in preparing ultra-high-performance concrete (UHPC): mixture design, characterization, and life-cycle assessment", *Resources, Conservation and Recycling*, 180, p.106136. https://doi.org/10.1016/j.resconrec.2021.106136

[41] Li, X., Lv, X., Zhou, X., Meng, W., and Bao, Y. (2022). "Upcycling of waste concrete in eco-friendly strain-hardening cementitious composites: mixture design, structural performance, and life-cycle assessment", *Journal of Cleaner Production*, 330, p.129911. https://doi.org/10.1016/j.jclepro.2021.129911

[42] Guo, P., Bao, Y. and Meng, W., 2021. Review of using glass in high-performance fiber-reinforced cementitious composites. *Cement and Concrete Composites*, 120, p.104032. https://doi.org/10.1016/j.cemconcomp.2021.104032

[43] Li, X., Xu, Z., Bao, Y., and Cong, Z. (2019). "Post-fire seismic behavior of two-bay two-story frames with high-performance fiber-reinforced cementitious composite joints", *Engineering Structures*, 183, pp.150-159. https://doi.org/10.1016/j.engstruct.2019.01.015

[44] Khan, M., Lao, J. and Dai, J.G., (2022). "Comparative study of advanced computational techniques for estimating the compressive strength of UHPC." *Journal of Asian Concrete Federation*, 8, pp.51-68. https://doi.org/10.18702/acf.2022.6.8.1.51

[45] Mahjoubi, S., Barhemat, R., Guo, P., Meng, W., and Bao, Y. (2021). "Prediction and multi-objective optimization of mechanical, economical, and environmental properties for strain-hardening cementitious composites (SHCC) based on automated machine learning and metaheuristic algorithms." *Journal of Cleaner Production*, 329, p.129665. https://doi.org/10.1016/j.jclepro.2021.129665

[46] Mahjoubi, S., Meng, W., and Bao, Y. (2022). "Auto-tune learning framework for prediction of flowability, mechanical properties, and porosity of ultra-high-performance concrete (UHPC)." *Applied Soft Computing*, 115, p.108182. https://doi.org/10.1016/j.asoc.2021.108182

[47] Mahjoubi, S., Barhemat, R., Meng, W., and Bao, Y. (2023). "AI-guided auto-discovery of low-carbon cost-effective ultra-high performance concrete (UHPC)." *Resources, Conservation and Recycling*, 189, p.106741. https://doi.org/10.1016/j.resconrec.2022.106741

[48] Li, V. C. (2019). *Engineered Cementitious Composites (ECC): Bendable Concrete for Sustainable and Resilient Infrastructure*, Springer. https://doi.org/10.1007/978-3-662-58438-5

[49] Deb, K., Pratap, A., Agarwal, S. and Meyarivan, T.A.M.T. (2002). "A fast and elitist multiobjective genetic algorithm: NSGA-II." *IEEE transactions on evolutionary*

computation, 6(2), pp.182-197. https://doi.org/10.1109/4235.996017

[50] FIU (Florida International University). (2019). "Public records requests related the bridge accident of March 15, 2018." https://facilities.fiu.edu/projects/BT-904-PRR.htm. Accessed January 22, 2022.

[51] Abaqus Group. (2011). "Abaqus 6.11." *Dassault Systemes Simulia Corp Providence*, RI, USA. http://193.136.142.5/v6.11/pdf_books/GUI.pdf. Accessed January 22, 2022.

[52] The Florida Department of Transportation (FDOT). (2019). "Denney Pate signed and sealed FIU bridge construction plans." https://cdn2.fdot.gov/fiu/13-Denney-Pate-signed-and-sealed-FIU-bridge-construction-plans.pdf. Accessed January 22, 2022.

[53] Jankowiak, T., and Lodygowski, T. (2005). "Identification of parameters of concrete damage plasticity constitutive model." *Foundations of Civil and Environmental Engineering*, 6(1), pp.53-69. https://www.infona.pl/resource/bwmeta1.element.baztech-article-BPP1-0059-0053

[54] Shamass, R., Zhou, X. and Alfano, G. (2015). "Finite-element analysis of shear-off failure of keyed dry joints in precast concrete segmental bridges. " *Journal of Bridge Engineering*, 20(6), p.04014084. https://doi.org/10.1061/(ASCE)BE.1943-5592.0000669

[55] Bao, Y., and Li, V. C. (2020). "Feasibility study of Lego-inspired construction with bendable concrete." *Automation in Construction*, 113, p.103161. https://doi.org/10.1016/j.autcon.2020.103161

[56] Haber, Z. B., De la Varga, I., Graybeal, B. A., Nakashoji, B., and El-Helou, R. (2018). "Properties and behavior of UHPC-class materials (No. FHWA-HRT-18-036)." *Office of Infrastructure Research and Development*, Federal Highway Administration, United States. https://rosap.ntl.bts.gov/view/dot/37528. Accessed January 22, 2022.

[57] Russell, H. G., Graybeal, B. A., and Russell, H. G. (2013). "Ultra-high performance concrete: A state-of-the-art report for the bridge community. (No. FHWA-HRT-13-060)" *Office of Infrastructure Research and Development*, Federal Highway Administration, United States. https://rosap.ntl.bts.gov/view/dot/26387. Accessed January 22, 2022.

[58] Yang, I.-H., Joh, C., and Kim, B.-S. (2012). "Flexural response predictions for ultra-high-performance fibre-reinforced concrete beams." *Magazine of Concrete Research*, 64(2), pp.113-127. https://doi.org/10.1680/macr.10.00115

[59] ACI Committee 318, (2005). "Building code requirements for structural concrete (ACI 318-05) and Commentary (318R-05)." *American Concrete Institute*, Farmington Hills, MI, USA. https://www.concrete.org/publications/internationalconcreteabstractsportal/m/details/id/14250

[60] Wtaife, S. A. M. (2019). "Design and Analysis of Fiber Reinforced Concrete Structure for Transportation Infrastructures." *Doctoral dissertation*. http://hdl.handle.net/11141/2808

[61] Zhou, J., Li, M., Ye, G., Schlangen, E., van Breugel, K., and Li, V. C. (2008). "Modelling the performance of ECC repair systems under differential volume changes." *In Concrete Repair, Rehabilitation and Retrofitting II*, pp.381-382. CRC Press. http://acemrl.engin.umich.edu/wp-content/uploads/sites/412/2018/10/14-zhou-eccrepair-2008.pdf

[62] Fischer, G., Stang, H., and Dick-Nielsen, L. (2007). "Initiation and development of cracking in ECC materials: Experimental observations and modeling." In *Proceedings of the 6th international conference on fracture mechanics of concrete and concrete structures*, 3, pp.1517-1522. https://framcos.org/FraMCoS-6/333.pdf

[63] Graybeal, B. A., and Baby, F. (2013). "Development of direct tension test method for ultra-high-performance fiber-reinforced concrete." *ACI Materials Journal*, 110(2), p.117. https://doi.org/10.14359/51685532

[64] Ranade, R., Li, V.C., Stults, M.D., Heard, W.F. and Rushing, T.S. (2013). "Composite properties of high-strength, high-ductility concrete. " *ACI Materials Journal*, 110(4), pp.413-422. http://acemrl.engin.umich.edu/wp-content/uploads/sites/412/2018/10/Composite-Properties-of-High-Strength-High-Ductility-Concrete.pdf

[65] Zhan, K., Yu, J., Wang, Y. and Yu, K. (2017). "Development of cementitious composites with tensile strain capacity up to 10%." *In RILEM Bookseries SHCC 2017: Strain-Hardening Cement-Based Composites*, pp.147-153. Springer, Dordrecht. https://doi.org/10.1007/978-94-024-1194-2_17

[66] Ding, Y., Yu, J., Yu, K. and Xu, S.L. (2018). "Basic mechanical properties of ultra-high ductility cementitious composites: From 40 MPa to 120 MPa. " *Composite Structures*, 185, pp.634-645. https://doi.org/10.1016/j.compstruct.2017.11.034

[67] Yu, K., Wang, Y., Yu, J. and Xu, S. (2017). "A strain-hardening cementitious composites with the tensile capacity up to 8%." *Construction and Building Materials*, 137, pp.410-419. https://doi.org/10.1016/j.conbuildmat.2017.01.060

[68] Wille, K., El-Tawil, S., & Naaman, A. E. (2014). "Properties of strain hardening ultra high performance fiber reinforced concrete (UHP-FRC) under direct tensile loading." *Cement and Concrete Composites*, 48, pp.53-66. https://doi.org/10.1016/j.cemconcomp.2013.12.015

[69] Hung, C. C., Lee, H. S., and Chan, S. N. (2019). "Tension-stiffening effect in steel-reinforced UHPC composites: constitutive model and effects of steel fibers, loading patterns, and rebar sizes." *Composites Part B: Engineering*, 158, pp.269-278. https://doi.org/10.1016/j.compositesb.2018.09.091

[70] Shafieifar, M., Farzad, M., and Azizinamini, A. (2017). "Experimental and numerical study on mechanical properties of ultra high performance concrete (UHPC)." *Construction and Building Materials*, 156, pp.402-411. https://doi.org/10.1016/j.conbuildmat.2017.08.170

[71] Wille, K., Naaman, A.E., El-Tawil, S. and Parra-Montesinos, G.J. (2012). "Ultra-high performance concrete and fiber reinforced concrete: Achieving strength and ductility without heat curing." *Materials and Structures*, 45(3), pp.309-324. https://doi.org/10.1617/s11527-011-9767-0

[72] Li, V.C., (2019). "High-performance and multifunctional cement-based composite material." *Engineering*, 5(2), pp.250-260. https://doi.org/10.1016/j.eng.2018.11.031

Supplementary Materials

Table S1. Suggested hazard values [S1]

Hazards considered	Hazard values		
	1	2	3
Scour; debris and ice; vessel collision; seismic liquefaction; settlement; flood	• Outside of a 500-year flood plain. • Seismic design category A (low probability of earthquake leading to liquefaction). • Low hurricane risk [3 s gust wind speed less than 145 kph]. • Over a non-navigable channel. • Located more than 800 km from coast. • No potential for scour. • No records of significant earthquake, floods, or storm surge.	• Outside of a 100-year flood plain. • Seismic design category B, C (moderate probability of earthquake leading to liquefaction). • Moderate hurricane risk [3 s gust wind speed within 145 ~ 210 kph]. • Navigable channel for mid-sized vessels. • Located more than 80 km from coast. • A rating of NBI Item 113 (scour) of 5 or higher. • Records of moderate earthquake, floods or storm surge.	• Within a 100-year flood plain. • Seismic design category D, E, F (high probability of earthquake leading to liquefaction). • Moderate hurricane risk [3 s gust wind speed more than 210 kph]. • Navigable channel for large vessels. • Located within 80 km from coast. • A rating of NBI Item 113 (scour) of 4 or lower. • Observed drift and debris at piers/abutment history of ice flows in waterway.
Seismic; fatigue; vehicle collision; overload; fire	• Seismic design category A (low probability of seismic damage). • No records of significant earthquake. • ADTT less than 5,000 (low probability of fatigue failure). • Not spanning over a roadway. • Located more than 32 km from heavy industry. • No history of overloads, collision, fire under the bridge.	• Seismic design category B, C (moderate probability of seismic damage). • Records of moderate earthquake. • ADTT less than 10,000 (moderate probability of fatigue failure); • Spanning over a roadway with ADTT less than 1,000. • Located more than 16 km from heavy industry. • History of moderate level of overloads, collision, fire under the bridge.	• Seismic design category D, E, F (high probability of seismic damage). • Records of significant earthquake. • ADTT more than 10,000 (high probability of fatigue failure). • Spanning over a roadway with ADTT more than 1,000. • Located less than 16 km from heavy industry. • History of high level of overloads, collision, fire under the bridge.

Note: ADTT = annual average daily truck traffic.

Table S2. Bridge importance factor [S2]

Importance factor	Criteria
0.75	• Bridge is located on local routes. • Replacement costs less than 5% of the total agency budget. • Bridge does not carry utility lines. • Average daily traffic is less than 10,000. • Detour length less than 5 km, or level of service on detour is A or B.
1.0	• Bridge is located on National Highway System (NHS) or state routes. • Replacement costs more than 5% and less than 25% of agency budget. • Bridge carries utility lines such as fiber optics, communication lines, or other low-risk utilities (colocation). • Average daily traffic is more than 10,000 and less than 50,000. • Detour length more than 5 km and less than 16 km, or level of service on detour is C or D.
1.25	• Bridge is located on evacuation routes, critical infrastructure, the Strategic Highway Network, or national network for trucks. • Replacement costs more than 25% of the agency budget. • Bridge carries utility lines such as electricity, gas, or other high-risk utilities (colocation). • Average daily traffic is more than 50,000. • Detour length more than 16 km, or level of service on detour is E or F.

Table S3. Basic restoration time [S2]

Affected area	Severity of the hazard			
	Low	Moderate	Severe	Catastrophic
Isolated	1 day	2 weeks	6 months	N/A
Local	3 days	6 months	9 months	N/A
Regional	1 week	9 months	12 months	24 months

Table S4. Adjustment factor α_1 [S2]

Adjustment factor, α_1	Disaster management practices
0.8	At least three of the following criteria: • Public extreme event preparedness educational programs, scheduled test, and drill programs. • Designated evacuation routes. • Designated shelters. • Extreme event management plans and designated centers. • First responders equipped with necessary tools and equipment to manage the post extreme event conditions. • On-call emergency contractors for incident management. • Local access to equipment, goods, and materials for minimal restoration. • Available modes of transportation for individuals: > 2 [8-km radius around the bridge]. • Access to number of emergency facilities (including emergency, hospital, gas stations): ≥ 20 [8-km radius around the bridge]. • A Level III or higher emergency response management (ERM)*.
1.0	Not meeting the above criteria

* Emergency response management levels [S3]: Level I = police officers directing traffic; Level II = traffic signals; Level III = dynamic traffic signal timing and ramp metering; Level IV = traffic cameras and variable message signs; Level V = intelligent transportation systems and advanced traveler information systems.

Table S5. Adjustment factor α_2 [S2]

Adjustment factor, α_2	Agency's contracting practices
1.0	No history of disruptive events
1.1	History of low event
1.2	History of moderate event
1.4	History of severe event
1.6	History of catastrophic event

Table S6. Adjustment factor α_b [S2]

Adjustment factor, α_b	Type of bridge*
1.00	Single-span bridges [up to 15-m span], or multiple simply supported spans.
1.15	Medium-size bridges [up to 50-m span], multiple continuous spans, movable bridges.
1.30	Large-span bridges [from 50-m to 150-m span].
1.50	Complex bridges [generally longer than 150-m span]

* Bridge categories from Pennsylvania Department of Transportation (2015) [S4].

Table S7. Discrete resilience ranking scale [S2]

Resilience value, R (%)	Resilience class
0 ~ 20	Non-resilient
21 ~ 40	Extremely low
41 ~ 60	Low
61 ~ 80	Moderate
81 ~ 90	High
91 ~ 100	Very high

Supplementary Materials References

[S1] Moon, F. L., Laning, J., Lowdermilk, D. S., Chase, S., Hooks, J., and Aktan, A. E. (2009). "A pragmatic risk-based approach to prioritizing bridges." *In Nondestructive Characterization for Composite Materials, Aerospace Engineering, Civil Infrastructure, and Homeland Security*, 7294, pp.166-176. https://doi.org/10.1117/12.816253

[S2] Minaie, E., and Moon, F. (2017). "Practical and simplified approach for quantifying bridge resilience." *Journal of Infrastructure Systems*, 23(4), p.04017016. https://doi.org/10.1061/(ASCE)IS.1943-555X.0000374

[S3] Freckleton, D., Heaslip, K., Louisell, W., & Collura, J. (2012). "Evaluation of resiliency of transportation networks after disasters." *Transportation Research Record*, 2284(1), pp.109-116. https://doi.org/10.3141/2284-13

[S4] Pennsylvania DOT. (2019). "PennDOT design manual, part 4 - Publication No.15M.", Harrisburg, PA. https://www.dot.state.pa.us/public/PubsForms/Publications/PUB%2015M.pdf. Accessed January 11, 2022.

Published online: 14 June 2023

Reference

1. Tan et al (2022) Optimizing high-performance fber-reinforced cementitious composites for improving bridge resilience and sustainability. J Infrastruct Preserv Resil 3:18. https://doi.org/10.1186/s43065-022-00067-0